

See discussions, stats, and author profiles for this publication at: <https://www.researchgate.net/publication/231645108>

# Self-Assembly of PTCDA Ultrathin Films on Graphene: Structural Phase Transition and Charge Transfer Saturation

ARTICLE *in* THE JOURNAL OF PHYSICAL CHEMISTRY C · NOVEMBER 2010

Impact Factor: 4.77 · DOI: 10.1021/jp1031674

---

CITATIONS

18

READS

19

## 3 AUTHORS, INCLUDING:



Xiaoqing Tian

Shenzhen University

10 PUBLICATIONS 98 CITATIONS

[SEE PROFILE](#)

# Self-Assembly of PTCDA Ultrathin Films on Graphene: Structural Phase Transition and Charge Transfer Saturation

X. Q. Tian, J. B. Xu,\* and X. M. Wang

Department of Electronic Engineering and Materials Science and Technology Research Center, The Chinese University of Hong Kong, Shatin, N.T., Hong Kong SAR, People's Republic of China

Received: April 8, 2010; Revised Manuscript Received: October 5, 2010

The self-assembly of perylene-3,4,9,10-tetracarboxylic dianhydride (PTCDA) on graphene with coverage in the range of 0.3–3 monolayers (MLs) is characterized by a DFT-based *ab initio* calculation method. For  $\alpha$  modification mode, with a critical thickness of 1 ML, the growth of PTCDA on graphene follows the Stranski–Krastanov (SK) mode. For  $\beta$  modification mode, the PTCDA can form two complete MLs on a graphene substrate. From the thermodynamic viewpoint,  $\alpha$  modification mode is more stable than  $\beta$  modification mode. At 1 ML, the PTCDA follows a planar configuration on graphene, which is also almost unperturbed by typical defects in the graphene sheet. The PTCDA adlayer remains its planar and continuous herringbone structure on graphene with three typical defects. For  $\alpha$  modification mode with 2 or 3 ML coverage, the molecular planes incline to the substrate plane with angles around 9° and 13°, respectively, which indicates that a bulk-like phase appears. This also enhances the lateral intrinsic charge transport characteristics. For  $\alpha$  modification mode, the total amount of charge transfer between PTCDA and graphene per  $5\sqrt{3} \times 5$  super cell at 2 MLs saturates with 0.42e, which is 0.1 and 0.06e larger than those of 1 and 3 MLs, respectively.

## 1. Introduction

The graphene sheet, a two-dimensional crystal constructed by  $sp^2$  hybridization of carbon atoms, has attracted significant attention due to its extremely high carrier mobility, ballistic charge transport characteristics, and quantum relativistic phenomena.<sup>1–8</sup> The band structure of single-layer graphene exhibits as circular cone near six corner points  $K$  ( $K'$ ) of its first Brillouin zone. The graphene sheet whose  $\pi$  and  $\pi^*$  bands of electrons intersect at the Dirac points has the zero band gap attribute of semiconductors or semimetals. The intrinsic zero band gap characteristic has limited the potential applications of graphene in future nanoelectronics. Chemical functionalization of graphene is perceived to effectively modulate the electronic structure of graphene to attain the intended properties which will be exploited for the potential applications of graphene in nanoelectronics.

Atomic doping of graphene by depositing potassium and gold atoms onto graphene could be used for *n*- and *p*-type graphene semiconductors, respectively,<sup>9,10</sup> and a superconducting phase could be obtained by Sn cluster decorating.<sup>11</sup> However, atomic doping could cause clustering of doping species, severe structural conformation, and defects in the graphene. Surface functionalization of graphene by organic molecules, especially aromatic molecule doping, is a feasible route to tackle these problems. Recently, 1,3,6,8-pyrenetetrasulfonic acid (TPA) functionalized single-layer graphene was experimentally demonstrated. And it was found that the interaction between a TPA and the graphene could induce *G*-band splitting.<sup>12</sup> Meanwhile, an *n*-type molecular semiconductor PTCDA was deposited onto the graphene surface at room temperature. It was found that the molecules possess long-range order with a herringbone arrangement. The molecular ordering is unperturbed by defects in the epitaxial graphene or atomic steps in the underlying SiC

surface.<sup>13</sup> In-situ low-temperature scanning tunneling microscopy (LT-STM) and high-resolution x-ray photoemission spectroscopy are used (HR-XPS) to study the growth of PTCDA thin films on epitaxial graphene (EG) on 6H-SiC(0001), and it was revealed that there is a weak charge transfer between PTCDA and EG.<sup>14</sup> PTCDA has also fallen into research interest because of its initial growth morphology and electronic structure on metal, insulator, and semiconductor surfaces.<sup>15–24</sup> One of PTCDA's derivatives, 3,4,9,10-perylene tetracarboxylic acid (PTCA), was used to functionalize graphene, and atomic layer deposition of dielectric Al<sub>2</sub>O<sub>3</sub> on graphene on a micrometer scale was achieved.<sup>25</sup>

Accordingly, a stable and uniform PTCDA functionalized graphene may provide new opportunities for graphene-based electronics. However, the growth and doping mechanisms have yet to be elucidated. Here, we use state-of-the-art first principles technique to address the doping effect and growth mechanism of PTCDA on graphene. Our calculated results of the optimized structures prove that the well-ordered PTCDA monolayers naturally self-assemble on single-layer graphene, and the formation of herringbone orientation is attributed to the densely disposed intermolecular hydrogen bonds. In order to better understand the intriguing interfacial features, typical defects of graphene are considered. And it is found that they render very limited conformation to the monolayer, which is in good agreement with experiment.<sup>13</sup> We also find that the growth of PTCDA monolayers obeys the SK mode and a phase transition appears when the coverage approaches 2–3 MLs. Meanwhile, the calculation of band structure shows that the functionalized graphene behaves as *p*-type semiconductor and possesses an intrinsic band gap. This study ameliorates the understanding of organic ultrathin layers on graphene, and may inspire further design and fabrication of graphene-based devices.

\* To whom correspondence should be addressed. E-mail: jb.xu@ee.cuhk.edu.hk.

## 2. Computational Method

The calculations are performed within the Vienna *ab initio* simulation package (VASP).<sup>26</sup> The electron–ion interaction is described by the PAW method.<sup>27</sup> The plane-wave basis set cutoff used is 29.40 Ry. Local density approximation (LDA) is better than generalized gradient approximations (GGA) in weak binding systems.<sup>28,29</sup> Therefore, LDA is used. Our calculated graphite lattice constants are  $a = 2.445 \text{ \AA}$  and  $c = 6.627 \text{ \AA}$ , in good agreement with experimental values  $a = 2.462 \text{ \AA}$  and  $c = 6.710 \text{ \AA}$ . But LDA does not take into account the van der Waals interactions, and the ability to match the experimental interlayer spacing is due to a coincidental cancellation of errors. In order to better understand the growth process, we also conduct molecular mechanics (MM) calculations.<sup>30,31</sup> MM<sup>+</sup> force field, which is improved from MM2, is used in MM calculations. Another method to take into account the van der Waals interactions is to use DFT plus a long-range dispersion term.<sup>32,33</sup> Graphene  $5\sqrt{3} \times 8$  single-layer is used as substrate to simulate PTCDA molecule adsorption at single molecular level, which also corresponds to 0.3 ML adlayer, while a graphene  $5\sqrt{3} \times 5$  single-layer plus two molecules are used to simulate PTCDA monolayer adsorption. The molecule and graphene atoms are allowed to relax until residual forces in all directions are less than 20 meV/ $\text{\AA}$ . A 1.8-nm vacuum layer is used to eliminate the longitudinal interactions between super cells. The  $4 \times 4 \times 1$  and  $4 \times 6 \times 1$  Monkhorst-Pack  $k$ -point meshes are used for low and high coverage cases, respectively.

For PTCDA, 0.3 ML adlayer on graphene, nine adsorption configurations with different orientations are considered. The adsorption energy is calculated by the following equation:

$$E_{\text{ad}}^0 = -(E - E_0 - E_{\text{molecule}}) \quad (1)$$

where  $E$  is the total energy of the single-layer graphene with the molecule;  $E_{\text{molecule}}$  is the chemical potential of the molecule; and  $E_0$  is the total energy of pristine single-layer graphene.

## 3. Results and Discussion

**3.1. Adsorption of PTCDA on Graphene at Single Molecule Level.** The structural optimization result for most stable adsorption mode is shown in Figure 1. The single PTCDA molecule adsorption on graphene is thermodynamically stable under this structure due to its adsorption energy is  $E_{\text{ad}}^0 = 1.20 \text{ eV}$  and around 0.06–0.25 eV larger than those under other configurations. The vertical distance (averaged to each atom) between PTCDA and graphene is 3.11  $\text{\AA}$ . To investigate the PTCDA doping effects on graphene, the band structure for isolated PTCDA on graphene is shown in Figure 2. The Dirac energy level  $E_D$  is 160 meV higher than the Fermi level, and the band gap is 136 meV. As a result, PTCDA functionalized graphene shows *p*-type semiconductor characteristics. Furthermore, each PTCDA molecule gains 0.30 electrons from graphene.

**3.2. Adsorption of PTCDA Monolayer on Graphene.** The PTCDA monolayer (ML) on single-layer graphene is simulated by two molecules on each graphene  $5\sqrt{3} \times 5$  super cell. From experiments,<sup>34,35</sup> the unit cell parameters of the monolayer are  $a = 19.5 \text{ \AA}$  and  $b = 13.2 \text{ \AA}$ . Graphene  $5\sqrt{3} \times 5$  super cell with  $a = 21.175 \text{ \AA}$ ,  $b = 12.225 \text{ \AA}$  is the closest geometry to the experimental unit cell. Actually, there are other close unit cells such as graphene  $4\sqrt{3} \times 6$  and  $4\sqrt{3} \times 5$ . Nevertheless, for graphene  $4\sqrt{3} \times 6$ , the PTCDA monolayer cannot constitute a full C–H…O hydrogen bond network, especially in the  $b$

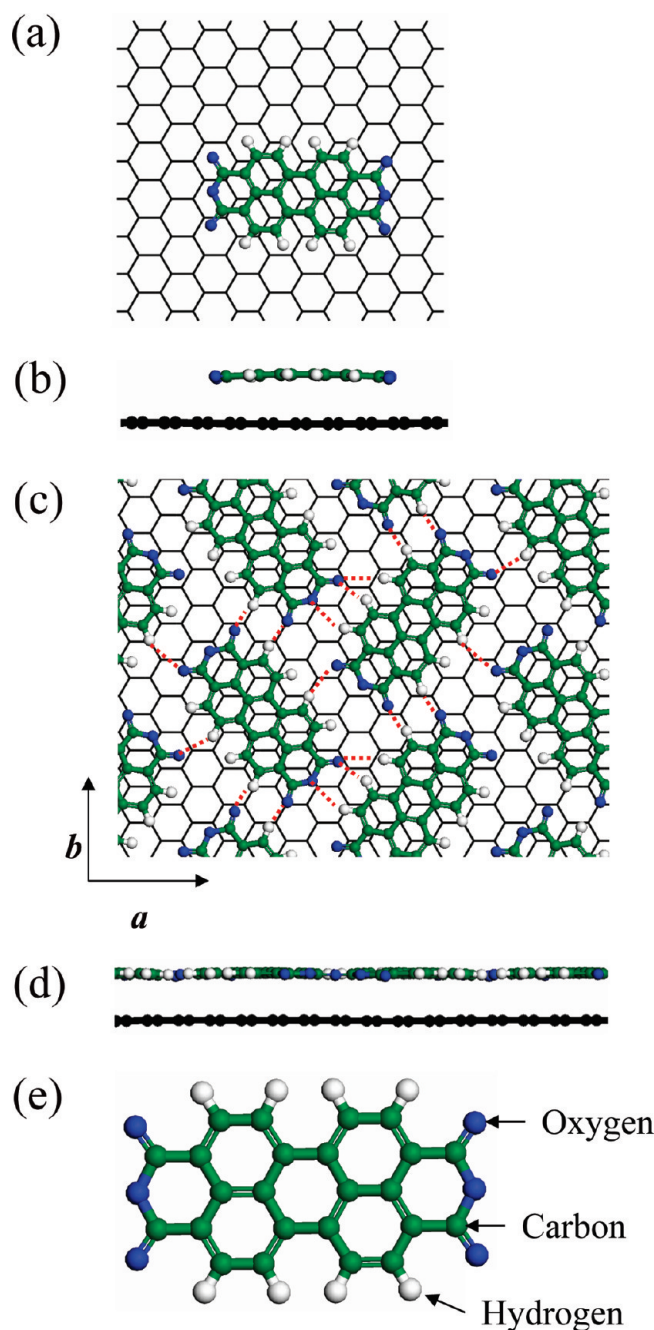


**Figure 1.** Calculated structures of PTCDA on graphene in different areal concentrations: (a) top view and (b) side view of 1/3 ML; (c) top view and (d) side view of 1 ML. (e) Structure of PTCDA molecule. Oxygen atoms are blue, hydrogen atoms are white, carbon atoms of PTCDA are green, and carbon atoms of graphene are black. Red dashed lines are hydrogen bonds.

direction with neighboring C…O distance around 5.10  $\text{\AA}$ . To form a good hydrogen bond, the C…O distance should be smaller than 4.0  $\text{\AA}$ .<sup>36–38</sup> However, for graphene  $4\sqrt{3} \times 5$ , the distance among atoms in neighboring molecules is too small, and the molecule will be decomposed after structural optimization. The laterally intermolecular interaction energy averaged to each molecule is defined by the following:

$$E_{\text{HB}} = -(E - 2E_{\text{molecule}})/2 \quad (2)$$

where  $E$  is the total energy of the molecular monolayer, which is composed of two molecules per supercell, and  $E_{\text{molecule}}$  is the

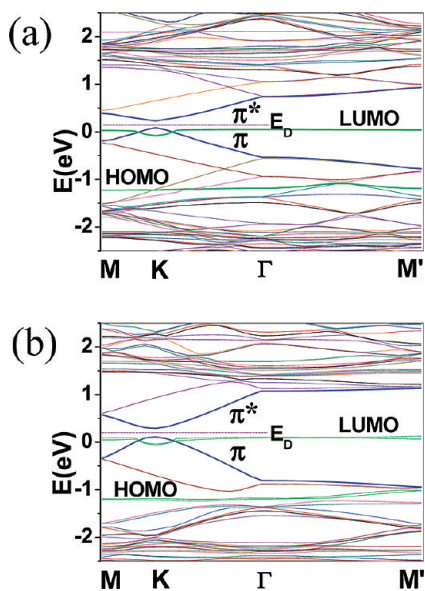


**Figure 2.** Band structure of PTCDA-doped graphene in different areal concentrations: (a) 0.3 ML and (b) 1 ML.

energy of the isolated molecule. For isolated PTCDA molecular monolayer, the intermolecular interaction energy is  $E_{HB} = 0.78$  eV, which is contributed from the intermolecular hydrogen bonds. Compared to single PTCDA adsorption energy 1.20 eV,  $E_{HB}$  is around 35% smaller.

The structural optimization for PTCDA monolayer on single-layer graphene is shown in Figure 1, parts (c) and (d). The average distance between the PTCDA monolayer and the graphene is 3.21 Å, which is 0.1 Å larger than the distance of the single PTCDA molecule adsorbed on graphene. The monolayer rumpling is within 0.23 Å and the graphene rumpling is no more than 0.10 Å. PTCDA molecules are arranged as a herringbone packing to keep totally 10 hydrogen bonds among each molecule and neighboring molecules. The adsorption energy of the monolayer layer averaged to each molecule is calculated by:

$$E_{ad}^1 = -(E - E_0 - E_{monolayer})/2 \quad (3)$$

where  $E$  is the total energy of the single-layer graphene with monolayer adsorption;  $E_{monolayer}$  is the total energy of monolayer; and  $E_0$  is the total energy of pristine single-layer graphene. The adsorption energy for each molecule is  $E_{ad}^1 = 0.83$  eV, around 35% smaller than  $E_{ad}^0$ . For PTCDA monolayer on graphene,  $E_{HB}$  is comparable to  $E_{ad}^1$ . Since  $E_{HB}$  is the in-plane intermolecular energy, it plays the role as driving force for PTCDA to grow in plane and on top of substrate together with  $E_{ad}^1$ . These two interactions: in plane intermolecular interaction and molecule–substrate interaction help PTCDA to form a complete monolayer on graphene substrate. The relative energy stability for PTCDA monolayer to isolated PTCDA molecule adsorption is  $E_{ad}^1 + E_{HB} - E_{ad}^0 = 0.41$  eV averaged to each molecule.

Its corresponding band structure is shown in Figure 2(b). Each molecule obtains 0.16e from graphene and is around 57% of single molecular charge transfer between PTCDA and graphene, which indicates that the molecule–substrate interaction is suppressed by increasing the coverage. The gained charge from graphene substrate is mainly localized around the carbonyl group of PTCDA. When PTCDA establishes hydrogen bonds with its 6 neighbors, its carbonyl group's chemical activity has been

weakened. This results in the suppression of charge acceptor ability of PTCDA monolayer in contrast to the isolated PTCDA molecule. Similar to the variation of charge acceptor ability, the adsorption energy for PTCDA on graphene is reduced due to the reduction of chemical activity by the formation of the dense hydrogen bond network.

Although the charge transfer for each molecule is decreased, the averaged graphene surface charge density increases by 70%. The band gap of graphene is 182 meV. Therefore, by increasing the coverage of PTCDA monolayer, the band gap opening is enhanced.

### 3.3. PTCDA Monolayer Growth on Defect Functionalized Graphene.

To further investigate the graphene substrate interaction with PTCDA adlayer, three typical graphene defects: Stone Wales defect (SW), single vacancy (SV), and double vacancies (DV) in 1% concentration are considered.

The structural optimization for PTCDA adlayer on graphene with SW defect is shown in Figure 3, parts (a) and (b). Although the adlayer–substrate interaction has caused a strong conformation in graphene, the PTCDA adlayer retains its planar geometry. The averaged adsorption energy for each molecule is 1.03 eV, so the SW defect can enhance the interaction between adlayer and substrate. The average distance between them is 3.22 Å. But the closest distance between oxygen atom and graphene atoms is reduced to 3.05 Å, compared to 3.22 Å for adlayer on pristine graphene. So it can be understood why the averaged distance is unchanged, but the adsorption energy is increased by 0.2 eV. The rumpling of PTCDA monolayer is within 0.28 Å and the rumpling of graphene is 0.78 Å. Compared to the adlayer on pristine graphene, the PTCDA adlayer adsorption induced the rumpling increment in graphene is around fourteen times that of PTCDA adlayer.

Figure 3(c),(d) shows the structural optimization for PTCDA monolayer on graphene with SV defect. The vertical distance between PTCDA and graphene is 3.21 Å. The adsorption energy is  $E_{ad} = 0.96$  eV, averaged to each molecule, which is 0.13 eV larger than that on pristine graphene. The first closest distances between the oxygen atom and the graphene atoms are reduced to 3.19 Å in comparison to that of a single monolayer on graphene, 3.22 Å. The monolayer rumpling on a single vacancy functionalized graphene sheet is almost the same as that for a monolayer on pristine one, but graphene rumpling is strongly increased by 0.38 Å.

The structural optimization for PTCDA adlayer on graphene with DV defect is shown in Figure 3, parts (e) and (f). The vertical distance between PTCDA and graphene is 3.21 Å. The adsorption energy is 0.95 eV, averaged to each molecule, which is 0.12 eV larger than that on pristine graphene. The first closest distance between oxygen atom and graphene is reduced to 3.19 Å. Both the molecular and graphene's rumpling are compared to PTCDA adlayer on pristine graphene.

To summarize, defects in graphene have very limited perturbation effects on the structural conformation of PTCDA monolayer. The PTCDA adlayer remains its planar structure on the defect areas and full hydrogen bonding network between neighboring molecules. These results corroborate experimental results that PTCDA monolayer long-range ordering is unperturbed by the defects in graphene substrate.<sup>13</sup>

### 3.4. PTCDA Bilayer Growth on Graphene.

The PTCDA multiple-layers on graphene are further investigated. The adsorption energies for different coverages are summarized in Table 1. To start with, eight configurations for PTCDA bilayer on single-layer graphene are considered, with four typical optimized structures as shown in Figure 4.

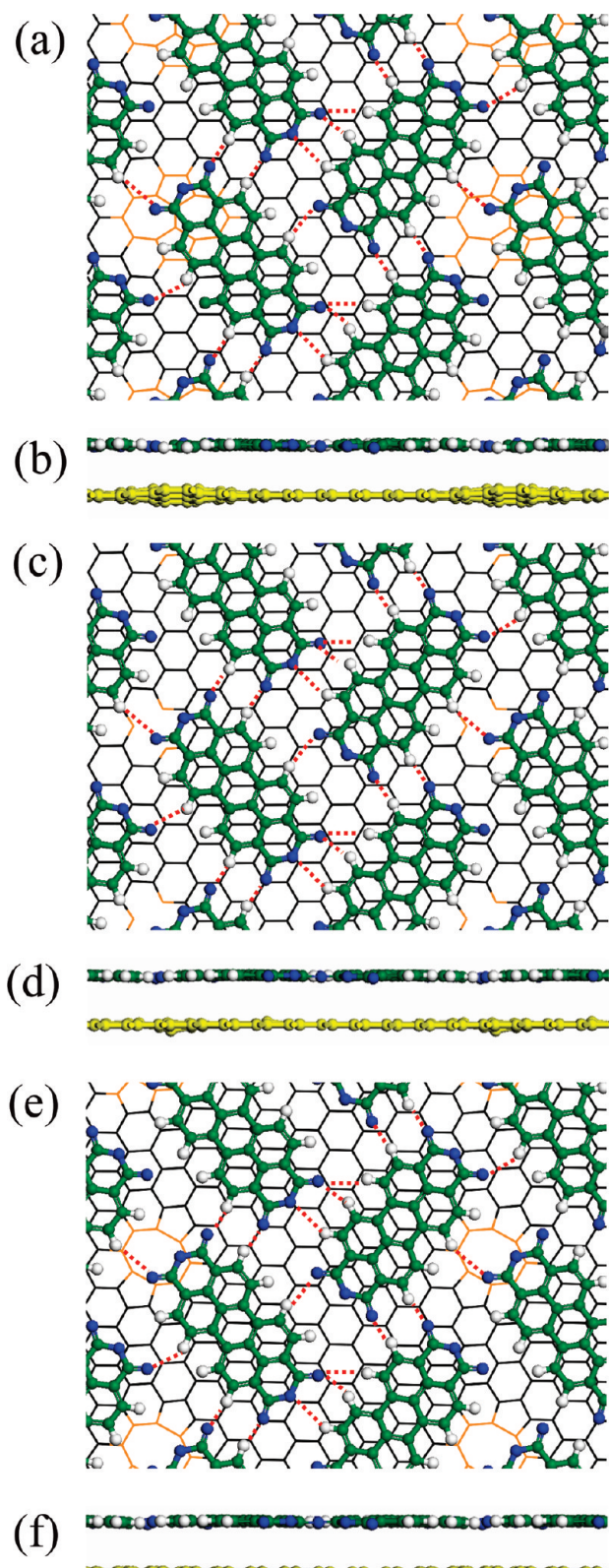


**Figure 3.** Calculated structures of PTCDA ML around three typical defected areas: (a) and (b) SW defect; (c) and (d) SV defect; and (e) and (f) DV defect. Defected areas are brown. Red dashed lines are hydrogen bonds.

The adsorption energy of the second layer averaged to each molecule is calculated by the following:

$$E_{ad}^2 = -(E - E^1 - E_{monolayer})/2 \quad (4)$$

**TABLE 1: Evolution of Intermolecular and Molecule–Substrate Interaction Energies**

	$E_{HB}$	$E_{ad}^{0}$	$E_{ad}^{1}$	$E_{ad}^{2,\alpha}$	$E_{ad}^{2,\beta}$	$E_{ad}^{3,\alpha}$	$E_{ad}^{3,\beta}$
energy (eV)	0.78	1.20	0.83	0.75	0.73	0.88	0.68

where  $E$  is the total energy of the single layer graphene with bilayer PTCDA adsorption;  $E_{monolayer}$  is the total energy of isolated monolayer; and  $E^1$  is the total energy of single-layer graphene with monolayer adsorption.

Subsequently, the adsorption energy of the third layer averaged to each molecule is calculated by the following:

$$E_{ad}^3 = -(E - E^2 - E_{monolayer})/2 \quad (5)$$

where  $E$  is the total energy of the single layer graphene with trilayer PTCDA adsorption;  $E_{monolayer}$  is the total energy of the isolated PTCDA monolayer; and  $E^2$  is the total energy of single-layer graphene with bilayer adsorption.

For type I configuration, as shown in Figure 4, parts (a) and (b), the relative shift of the second layer to the first layer is 1.62 Å, and the shift direction is neither along  $a$  nor  $b$ , with an angle around  $-45^\circ$  to  $a$ . In this case, the stacking of right molecule in the top layer to the bottom layer is similar to the Bernal stacking of graphite  $\pi$  electrons, and the stacking of the left molecule in the top layer to the bottom layer slightly differs from the Bernal stacking. Hence it is expected this configuration may have a larger adsorption energy contributed from  $\pi$  electron interaction of the two PTCDA monolayers. The adsorption energy contributed from the second layer, averaged to each molecule ( $E_{ad}^2$ ) is 0.65 eV. The adsorbed two layer planes are titled around  $3^\circ$  relative to the graphene plane.  $E_{ad}^2$  is smaller than that of the single monolayer-substrate absorption energy  $E_{ad}^1 = 0.83$  eV, and the intermolecular lateral interaction energy  $E_{HB} = 0.78$  eV. So the adsorption of the top monolayer has a minor effect on the bottom monolayer.

Type II configuration is shown in Figure 4, parts (c) and (d). The adsorption energy of the second monolayer PTCDA is  $E_{ad}^2 = 0.29$  eV. The top monolayer has no lateral shift relative to the bottom monolayer. The two layer planes are nearly parallel to the graphene plane, with an angle around  $1^\circ$  respect to the graphene one.  $E_{ad}^2$  is fairly smaller than  $E_{ad}^1$  and  $E_{HB}$ . So the adsorption of the top monolayer has negligible effect on the bottom monolayer.

The optimized structure of type III configuration ( $\alpha$  modification) is shown in Figure 4, parts (e) and (f). The second monolayer has a shift of 2.12 Å with respect to the first layer along  $a$  direction. The PTCDA adsorption energy contributed from the second layer is  $E_{ad}^{2,\alpha} = 0.75$  eV.  $E_{ad}^{2,\alpha}$  is slightly larger than  $E_{HB}$  and is close to  $E_{ad}^{1,\alpha}$ . Therefore, the adsorption of the top layer can affect the bottom layer. The top and bottom layer planes are slanted at  $10^\circ$  and  $8^\circ$  angles, respectively, relative to the graphene plane. There are 8 interlayer hydrogen bonds between the top and bottom layers, which contribute to the adsorption energy and ensure the adsorption configuration more stable. We also consider the type III configuration, with the top layer having a shift of 1.85 and 2.41 Å relative to the first layer along  $a$  direction, respectively. It is found that their adsorption energies are smaller than those in the type III configuration with 2.12 Å shift. The top PTCDA layer has in total 8 hydrogen bonds with the bottom layer, which presumably drives the PTCDA phase transition from surface phase to bulk-like phase. Each PTCDA of the bottom layer gains 0.15e from graphene, while the top layer attains 0.06e from graphene.

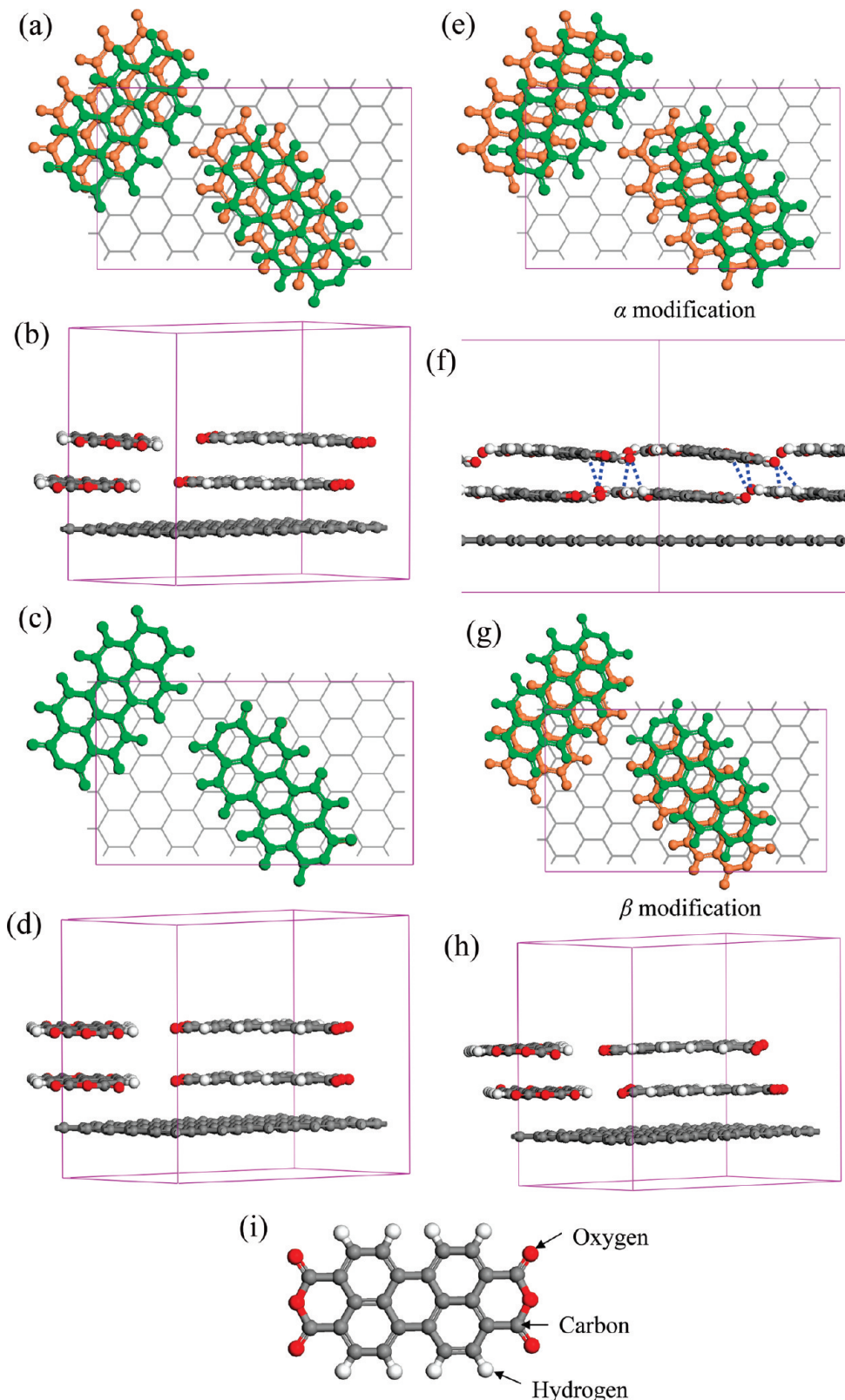


**Figure 4.** Optimized configurations of PTCDA bilayer on graphene with four typical configurations: (a) and (b) type I; (c) and (d) type II; (e) and (f)  $\alpha$  modification; (g) and (h)  $\beta$  modification. (i) structure of PTCDA molecule. In top view, top molecule is brown and bottom is green. In side view, oxygen atoms are red, hydrogen atoms are white, and carbon atoms are gray. Blue dashed lines are interlayer hydrogen bonds.

The optimized structure of type IV configuration ( $\beta$  modification) is depicted in Figure 4, parts (g) and (h). The second layer has a shift of 2.00 Å relative to the first layer along *b* direction. Its adsorption energy is  $E_{ad}^{2,\beta} = 0.73$  eV. Type IV configurations, with a shift of 1.76 and 2.32 Å have also been calculated, and their adsorption energy is smaller than those with 2.00 Å

shift. Therefore, it is anticipated that  $\beta$  modification with 2.00 Å shift is thermodynamically stable.

So it is concluded that for PTCDA bilayer growth on graphene,  $\alpha$  modification is more thermodynamically stable than  $\beta$  modification, due to  $E_{ad}^{2,\alpha}$  larger than  $E_{ad}^{2,\beta}$ . MM calculation also confirms that the  $\alpha$  modification is more stable than  $\beta$

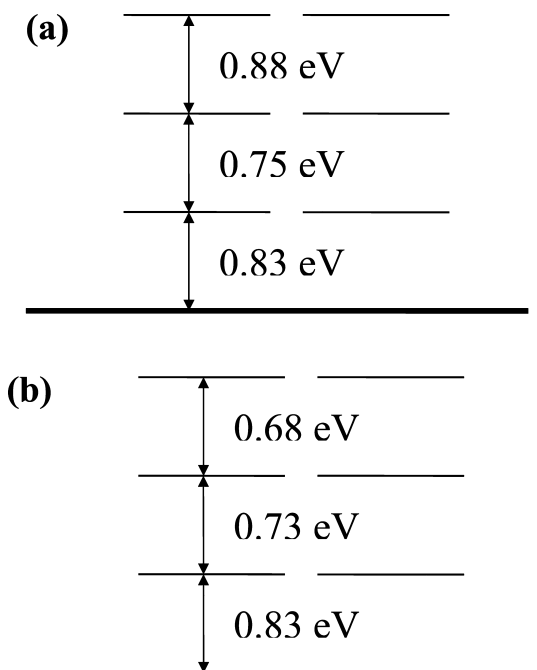


**Figure 5.** Comparison of out-plane adsorption energy for three layers (a)  $\alpha$  modification; and (b)  $\beta$  modification. Thick line stands for graphene substrate and each two in-plane thin lines stand for PTCDA monolayer.

modification with an energy preference of 50 meV. The comparison for out-plane adsorption energy of different PTCDA layers is shown in Figure 5. For  $\alpha$  modification mode, the  $E_{ad}^{2,\alpha}$  is smaller than  $E_{ad}^{1,\alpha}$  by 0.08 eV, so the growth of the full first layer is preferable to the incomplete first layer with a partially grown second layer on the top thermodynamically. Similarly, this comparison is applicable for  $\beta$  modification mode. For initial growth stage of PTCDA on graphene, the PTCDA can form a complete first monolayer on graphene substrate, and this is in agreement with experimental findings.<sup>13,14</sup>

**3.5. PTCDA Trilayer Growth on Graphene.** Subsequently, PTCDA trilayer growth on graphene with both  $\alpha$  and  $\beta$  modifications are investigated, with the optimized structures shown in Figure 6.

For  $\alpha$  modification of 2.15 Å, the adsorption energy contributed by the third layer, averaged to each molecule ( $E_{ad}^{3,\alpha}$ ) is 0.88 eV. Obviously,  $E_{ad}^{3,\alpha}$  is larger than both  $E_{ad}^{2,\alpha}$  and  $E_{HB}$ . Hence it is expected that the adsorption of the third PTCDA monolayer will introduce structural conformation in the bottom bilayer. The top, middle, and bottom layer planes have tilted angles around 15°, 13°, and 10°, relative to the graphene plane, respectively. So PTCDA molecules with high coverage tend to incline relative to graphene substrate, which eventually improves the lateral transport properties and is useful for organic transistors. The top layer has 14 hydrogen bonds with the middle layer in each super cell, which contributes to the adsorption energy and enlarges the inclination angles of the molecular planes relative to the substrate. Besides, the dense intermolecular hydrogen bonds can help to drive the phase transition from surface phase to bulk-like phase to release the free energy. Each bottom PTCDA gains 0.15e from graphene, while the middle and top attains 0.02 and 0.01e, respectively from graphene, and the total amount of charge transfer of 0.36e is less than that of 0.42e in bilayer. Therefore, it is awaited that the total charge transfer saturates in the bilayer configuration. For  $\alpha$  modification, 1.90 and 2.38 Å shifts are also calculated, with the adsorption energies smaller than that with 2.15 Å shift. On the

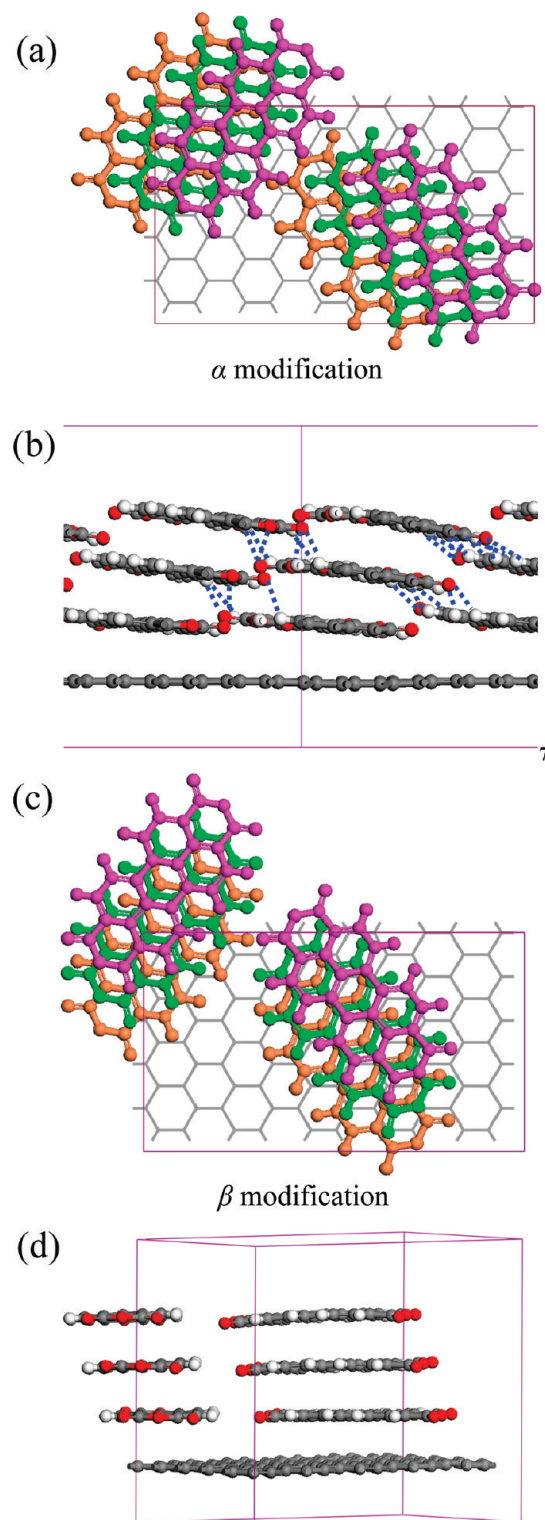


**Figure 6.** Optimized configurations of PTCDA trilayer on graphene: (a) and (b)  $\alpha$  modification; (c) and (d)  $\beta$  modification. For the top view, the top molecule is pink, middle is brown, and bottom is green. Blue dashed lines are interlayer hydrogen bonds.

basis of the analysis of out-plane adsorption energy as shown in Figure 5 (a),  $E_{ad}^{3,\alpha}$  is larger than  $E_{ad}^{2,\alpha}$ , so the growth of island on the top of the incomplete second layer is more stable than the growth of a complete second layer thermodynamically. For  $\alpha$  modification mode, PTCDA molecules do not form a second complete monolayer on graphene, and the growth of PTCDA follows 3D island growth mode,<sup>39</sup> when the coverage is larger than 1 ML. So the growth of PTCDA on graphene follows SK

mode (layer plus island). Now, we shall turn back to both eqs 4 and 5 for the variation of in-plane intermolecular energy, or in other words, the in-plane hydrogen bond energy deformation. Both eqs 4 and 5 do not clearly include the in-plane intermolecular energy, and assume it to be a constant as that of an isolated monolayer. Actually, the in-plane intermolecular energy is decreased as the coverage is increased, due to the deformation of the planarity of PTCDA monolayer. If the variation of in-plane intermolecular energy of the  $n^{\text{th}}$  layer for each molecule (averaged by 2) is  $-\Delta$ , then the actual adsorption energy of the  $n^{\text{th}}$  layer will be  $E_{\text{ad}}^{n,\alpha} + \Delta$  or  $E_{\text{ad}}^{n,\beta} + \Delta$ . For example, the  $-\Delta$  of the second and third layer of PTCDA is  $-0.05$  and  $-0.11$  eV, respectively, for  $\alpha$  modification mode. For  $\beta$  modification mode, the deformation of PTCDA planarity is very limited, so the  $-\Delta$  is probably negligible. But from the thermodynamic point of view, we should take into account of both  $E_{\text{ad}}^{n,\alpha} + \Delta$  and  $-\Delta$  to analyze the growth mode, so the net value will be  $E_{\text{ad}}^{n,\alpha}$  for analyzing the growth mode.

For trilayer with  $\beta$  modification growth, the adsorption energy of  $1.96$  Å shift is  $E_{\text{ad}}^{3,\beta} = 0.68$  eV, which is larger than that of both  $1.76$  Å and  $2.22$  Å. The PTCDA molecular planes are tilted around  $3^\circ$  respective to graphene substrate. There exists no hydrogen bond among PTCDA monolayers. By comparison of out-plane adsorption energy as shown in Figure 5(b),  $E_{\text{ad}}^{3,\beta}$  is smaller than  $E_{\text{ad}}^{2,\beta}$  by  $0.05$  eV, so the complete second layer is more stable than the partially grown third layer on the top of the incomplete second layer thermodynamically. For  $\beta$  modification growth, PTCDA could form a second complete layer on graphene.

Therefore, for PTCDA trilayer on graphene,  $\alpha$  modification is more stable than  $\beta$  modification, due to energy preference of  $0.20$  eV as shown in Table 1. From MM calculation, the  $\alpha$  modification is more stable than  $\beta$  modification due to energy preference of  $0.29$  eV.

#### 4. Conclusions

Electronic properties of PTCDA ultrathin-layer assembly on single-layer graphene are investigated by DFT based *ab initio* calculation techniques. PTCDA monolayers are deposited in a stable herringbone configuration on a graphene sheet. Typical defects in graphene substrate have very limited perturbation effects on structural planarity and continuity of PTCDA monolayer. The growth of PTCDA on graphene follows the SK mode. A distinctive phase transition from surface-phase to bulk-like phase appears, when the coverage reaches  $2\text{--}3$  MLs. In particular, at  $3$  MLs of coverage, the molecular planes of PTCDA have a larger inclined angle to graphene substrate, with the top monolayer at  $15^\circ$ , which is highly anticipated to affect the lateral charge transport characteristics, and be useful in organic transistors. Meanwhile, PTCDA molecules gain electrons from graphene, which clearly demonstrate *p*-type doping attributes. For bilayer PTCDA coverage, the total charge transfer between them per PTCDA molecule is  $0.42e$ , which is  $0.1e$  and  $0.06e$  larger than those in  $1$  and  $3$  ML coverage, respectively. Moreover, it introduces a direct band gap into the graphene sheet. These results are in agreement with experiment, and exhibit a progressive way of PTCDA growth on graphene. This approach presents a potential to explore self-assembled organic layers on graphene and paves the way for design of graphene-based nanoelectronics.

**Acknowledgment.** The technical assistance at the High Performance Computing Facilities of the Information Technology Service Center, The Chinese University of Hong Kong,

particularly, by Mr. Frank Ng and Mr. Stephen Chan, is gratefully acknowledged. This work is supported in part by the Research Grants Council of Hong Kong, particularly, via Grant Nos. CUHK2/CRF/08, and CUHK4179/10E. J.B.X. would like to thank the National Science Foundation of China for support, particularly, via Grant Nos. 60990314 and 60928009.

**Supporting Information Available:** (1) Evolution of in-plane intermolecular and molecule–substrate interaction energies calculated by MM. (2) Detailed information about charge transfer at PTCDA ultrathin film/graphene interface and the corresponding isosurface of charge difference distribution at different densities. (3) Optimized structures of PTCDA trilayer on graphene by MM. This material is available free of charge via the Internet at <http://pubs.acs.org>.

#### References and Notes

- (1) Novoselov, K. S.; Geim, A. K.; Morozov, S. V.; Jiang, D.; Zhang, Y.; Dubonos, S. V.; Grigorieva, I. V.; Firsov, A. A. *Science* **2004**, *306*, 666.
- (2) Castro Neto, A. H.; Guinea, F.; Peres, N. M. R.; Novoselov, K. S.; Geim, A. K. *Rev. Mod. Phys.* **2009**, *81*, 109.
- (3) Morozov, S. V.; Novoselov, K. S.; Katsnelson, M. I.; Schedin, F.; Elias, D. C.; Jaszczak, J. A.; Geim, A. K. *Phys. Rev. Lett.* **2008**, *100*, 016602.
- (4) Kudin, K. N.; Ozbas, B.; Schniepp, H. C.; Prud'homme, R.; Aksay, I. A.; Car, R. *Nano Lett.* **2008**, *8*, 36.
- (5) Park, C.-H.; Giustino, F.; Spataru, C. D.; Cohen, M. L.; Louie, S. G. *Nano Lett.* **2009**, *9*, 4234.
- (6) Pan, Y.; Zhang, H. G.; Shi, D. X.; Sun, J. T.; Du, S. X.; Liu, F.; Gao, H. *J. Adv. Mater.* **2009**, *21*, 2777.
- (7) Xiang, H.; Kan, E. J.; Wei, S. H.; Whangbo, M. H.; Yang, J. L. *Nano Lett.* **2009**, *9*, 4025.
- (8) Huang, B.; Liu, M.; Su, N. H.; Wu, J.; Duan, W. H.; Gu, B. L.; Liu, F. *Phys. Rev. Lett.* **2008**, *100*, 016602.
- (9) Ohta, T.; Bostwick, A.; Seyller, T.; Horn, K.; Rotenberg, E. *Science* **2006**, *313*, 951.
- (10) Gierz, I.; Riedl, C.; Starke, U.; Ast, C. R.; Kern, K. *Nano Lett.* **2008**, *8*, 4603.
- (11) Kessler, B. M.; Girit, C. Ö.; Zettl, A.; Bouchiat, V. *Phys. Rev. Lett.* **2010**, *104*, 047001.
- (12) Dong, X. C.; Shi, Y. M.; Zhao, Y.; Chen, D. M.; Ye, J.; Yao, Y. G.; Gao, F.; Ni, Z. H.; Yu, T.; Shen, Z. X.; Huang, Y. X.; Chen, P.; Li, L. J. *Phys. Rev. Lett.* **2009**, *102*, 135501.
- (13) Wang, Q. H.; Hersam, M. C. *Nat. Chem.* **2009**, *1*, 206.
- (14) Huang, H.; Chen, S.; Gao, X. Y.; Chen, W.; Wee, A. T. S. *Acad. Nano* **2009**, *3*, 3431.
- (15) Temirov, R.; Soubatch, S.; Luican, A.; Tautz, F. S. *Nature* **2006**, *444*, 350.
- (16) Du, S. X.; Gao, H. J.; Seidel, C.; Tsetseris, L.; Ji, W.; Kopf, H.; Chi, L. F.; Fuchs, H.; Pennycook, S. J.; Pantelides, S. T. *Phys. Rev. Lett.* **2006**, *97*, 156105.
- (17) Burke, S. A.; Ji, W.; Mativetsky, J. M.; Topple, J. M.; Fostner, S.; Gao, H.-J.; Guo, H.; Grüter, P. *Phys. Rev. Lett.* **2008**, *100*, 186104.
- (18) Jalkanen, J. P.; Zerbetto, F. J. *Phys. Chem. B* **2006**, *110*, 5595.
- (19) Swarbrick, J. C.; Rogers, B. L.; Champness, N. R.; Beton, P. H. *J. Phys. Chem. B* **2006**, *110*, 6110.
- (20) Ma, J.; Rogers, B. L.; Humphry, M. J.; Ring, D. J.; Goretzki, G.; Champness, N. R.; Beton, P. H. *J. Phys. Chem. B* **2006**, *110*, 12207.
- (21) Yang, A.; Shipman, S. T.; Garrett-Roe, S.; Johns, J.; Strader, M.; Szymanski, P.; Muller, E.; Harris, C. *J. Phys. Chem. C* **2008**, *112*, 2506.
- (22) Eremchenko, M.; Schaefer, J. A.; Tautz, F. S. *Nature* **2003**, *9*, 602.
- (23) Kendrick, C.; Kahn, A. *J. Cryst. Growth* **1997**, *181*, 192.
- (24) Möbus, M.; Karl, N.; Kobayashi, T. *J. Cryst. Growth* **1992**, *116*, 495.
- (25) Wang, X. R.; Tabakman, S. M.; Dai, H. J. *J. Am. Chem. Soc.* **2008**, *130*, 8152.
- (26) Kresse, G.; Furthmüller, J. *Comput. Mater. Sci.* **1996**, *6*, 15.
- (27) Kresse, G.; Joubert, D. *Phys. Rev. B* **1999**, *59*, 1758.
- (28) Rochefort, A.; Wuest, J. D. *Langmuir* **2009**, *25*, 210.
- (29) Li, M. M.; Zhang, J.; Li, F. J.; Zhu, F. X.; Zhang, M.; Zhao, X. F. *Phys. Status Solidi C* **2009**, *6*, s90.
- (30) Shi, D. X.; Ji, W.; Lin, X.; He, X. B.; Lian, J. C.; Gao, L.; Cai, J. M.; Lin, H.; Du, S. X.; Lin, F.; Seidel, C.; Chi, L. F.; Hofer, W. A.; Fuchs, H.; Gao, H.-J. *Phys. Rev. Lett.* **2006**, *96*, 226101.
- (31) Ulbricht, H.; Moos, G.; Hertel, T. *Phys. Rev. Lett.* **2003**, *90*, 095501.
- (32) Feng, C.; Lin, C. S.; Fan, W.; Zhang, R. Q.; Van Hove, M. A. *J. Chem. Phys.* **2009**, *131*, 194702.

- (33) Chakarova-Kačk, S. D.; Schröder, E.; Lundqvist, B. I.; Langreth, D. C. *Phys. Rev. Lett.* **2006**, 96, 146107.
- (34) Kendrick, C.; Kahn, A.; Forrest, S. R. *Appl. Surf. Sci.* **1996**, 104/105, 586.
- (35) Hoshino, A.; Isoda, S.; Kurata, H.; Kobayashi, T. *J. Appl. Phys.* **1994**, 76, 4113.
- (36) Jiang, L.; Lai, L. H. *J. Biol. Chem.* **2002**, 277, 37732.
- (37) Scheiner, S.; Kar, T.; Gu, Y. L. *J. Biol. Chem.* **2001**, 276, 9832.
- (38) Desiraju, G. R. *Acc. Chem. Res.* **1996**, 29, 441.
- (39) Musolino, V.; Selloni, A.; Car, R. *Phys. Rev. Lett.* **1999**, 83, 3242.

JP1031674